15th World Congress on Computational Mechanics (WCCM-XV)
8th Asian Pacific Congress on Computational Mechanics (APCOM-VIII)
Virtual Congress: 31 July – 5 August 2022
S. Koshizuka (Ed.)

TIME DOMAIN SOUND FIELD ANALYSIS USING THE FINITE ELEMENT METHOD AND THE FAST MULTIPOLE BOUDARY ELEMENT METHOD

KAZUSHI FUKAZAWA[1], HITOSHI YOSHIKAWA[2] AND KAZUO KASHIYAMA[3]

[1] Graduate School of Civil, Human and Environmental Engineering, Chuo University
Kasuga 1-13-27, Bunkyo-ku, Tokyo 112-8521, JAPAN
a17.kfgc@g.chuo-u.ac.jp

[2] Graduate School of Informatics, Kyoto University
Yoshida-Honmachi, Sakyo-ku, Kyoto 606-8501, JAPAN
yoshikawa.hitoshi.5u@kyoto-u.ac.jp

[3] Department of Civil and Environmental Engineering, Chuo University
Kasuga 1-13-27, Bunkyo-ku, Tokyo 112-8521, JAPAN
kaz@civil.chuo-u.ac.jp

Key words: Finite Element Method, Boundary Element Method, Noise Barrier, Auralization

Abstract. *This paper presents a noise evaluation system based on acoustic wave theory. This paper utilizes two methods – the finite element method and the boundary element method using a fast multipole method, and compares the numerical results of the benchmark problem. In addition, we show the results using the analytical model of the complex shape based on standard specifications of noise barriers and discuss the difference of the numerical results and auralization results between the two methods.*

1 INTRODUCTION

Noise is one of the seven major types of pollution in Japan, and it has the highest number of complaints according to the results of a survey released by the Ministry of Internal Affairs and Communications in December 2021. Especially in urban areas, the evaluation of noise has been an urgent issue in the planning and designing of various constructions, such as roads, railways, and airports. In recent years, numerical simulation has been widely used based on geometric sound theory and wave sound theory as a noise evaluation method.

We have developed a sound field analysis method using the time-domain fast multipole boundary element method [1]. However, the boundary element method has a problem in that the material of the computational model is not considered strictly. Therefore, we aim to consider structure-borne sound transmission inside the computational model using the finite element method [2].

In this study, we show comparisons of the finite element method and the fast multipole boundary element method as a preliminary step of the purpose. At first, we perform benchmark analysis using a spherical wave because we verify the validity of the finite element analysis. Second, we perform acoustic analysis around sound barrier analysis that has complex shapes, and compare comparisons regarding visualization, qualitatively, and calculation costs.

2 NUMERICAL ANALYISIS METHOD

2.1 Governing equation and conditional expression

For the governing equation, the 3D unsteady wave equation is employed.

$$\frac{\partial^2 u}{\partial t^2}(\boldsymbol{x},t) = c^2 \frac{\partial^2 u}{\partial x^2}(\boldsymbol{x},t) \qquad \text{in} \quad D, \tag{1}$$

where $\boldsymbol{x}$ is the 3D spatial coordinate, D is the analysis domain, c is the sound speed, and u is the sound pressure. The following bounday conditions are employed.
Radiation condition：

$$u(\boldsymbol{x},t) = u_{\text{in}}(\boldsymbol{x},t), \qquad |\boldsymbol{x}| \to \infty, \;\; t > 0, \tag{2}$$

Dirichlet boundary condition：

$$u(\boldsymbol{x},t) = \hat{u}(\boldsymbol{x},t) \qquad \text{on} \quad \partial D_u, \tag{3}$$

Neumann boundary condition：

$$\frac{\partial u}{\partial n}(\boldsymbol{x},t) = -\frac{\rho}{Z_n}\frac{\partial u}{\partial t}(\boldsymbol{x},t) \qquad \text{on} \quad \partial D_{u'} \tag{4}$$

where ∂D_u, $\partial D_{u'}$ is each Dirichlet boundary condition, Neumann boundary condition. $\hat{u}$ is the existing sound pressure, n is the outward normal vector from the analysis domain, *rho* is the density, and Z_n is the normal acoustic impedance. This analysis assumes the incident wave is the orthogonal incident to the boundary plane.

$$\frac{\partial u}{\partial n}(\boldsymbol{x},t) = -\frac{\cos\theta}{c}\frac{1-\gamma}{1+\gamma}\frac{\partial u}{\partial t}(\boldsymbol{x},t) \qquad \text{on} \qquad \partial D_{u'} \tag{5}$$

where γ is the reflection coefficient. When γ is 1, the Neumann boundary condition is a perfect reflection, when γ is between 0 to 1, it is a random reflection, when γ is 1, it is a transmission condition[3]. Also, the initial conditions which are silent on the first step are the following.

$$u(\boldsymbol{x},t) = 0 \qquad \text{in} \quad D, \tag{6}$$

$$\frac{\partial u}{\partial t}(\boldsymbol{x},t) = 0 \qquad \text{in} \quad D, \tag{7}$$

2.2 Finite element method

The standard Galerkin's method is employed for equation (1). The following weak form is obtained.

$$\int_D u^* \frac{\partial^2 u}{\partial t^2} d\Omega + c^2 \int_D \frac{\partial u^*}{\partial x_i}\frac{\partial u}{\partial x_i} d\Omega = c^2 \int_{\partial D_{u'}} u^* \frac{\partial u}{\partial n} d\Gamma, \tag{8}$$

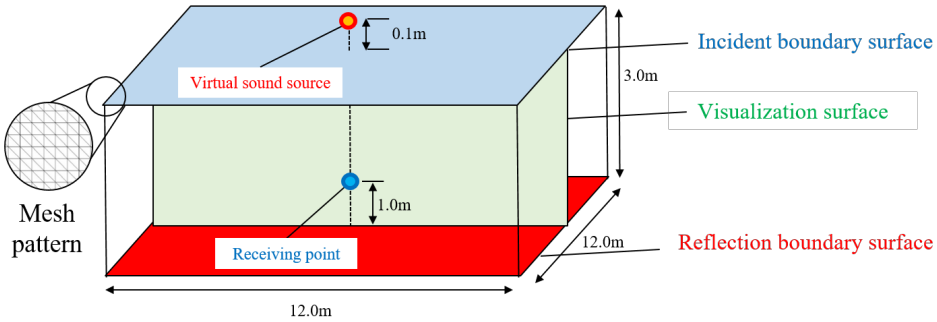

Figure 1: Computational model of benchmark problem

where x_i is the 3D spatial coordinate, u^* is the weight function of u. The subscript "e" indicates that the calculation is for each element. We use tetrahedral first-order elements for the spatial discretization for equation (8) to derive the following finite element equation.

$$\mathbf{M_e}\frac{\partial^2 u}{\partial t^2} + \mathbf{K_e}u = \mathbf{F_e} \tag{9}$$

where $\mathbf{M_e}$ is the mass matrix, $\mathbf{K_e}$ is the diffusion matrix, $\mathbf{F_e}$ is the boundary integral term. Each matrix could be as follows the integral.

$$\mathbf{M_e} = \int_D N^e_\alpha N^e_\beta d\Omega, \quad \mathbf{K_e} = \int_D \frac{\partial N^e_\alpha}{\partial x}\frac{\partial N^e_\beta}{\partial x} d\Omega, \quad \mathbf{F_e} = \int_{\partial D_{u'}} N^e_\alpha N^e_\beta \frac{\partial u}{\partial n} d\Gamma, \tag{10}$$

where N^e_α and N^e_β are each shape function of tetrahedral first-order elements. The discretization equation of the entire domain is derived by assembling the finite element equations obtained for each element.

The finite difference method is employed for the discretization in time.

2.3 Boundary element method

The boundary integrational equation can be derived from equations (1), (2), (6) and (7) as follows.

$$\begin{aligned}\frac{1}{2}u(\boldsymbol{x},t) = &\int_0^t \int_{\partial D} G(\boldsymbol{x}-\boldsymbol{y},t-s)\frac{\partial u}{\partial n}(\boldsymbol{y},s)d\Gamma ds \\ &- \int_0^t \int_{\partial D} \frac{\partial G}{\partial n}(\boldsymbol{x}-\boldsymbol{y},t-s)u(\boldsymbol{y},s)d\Gamma ds + u_{\text{in}}(\boldsymbol{x},t),\end{aligned} \tag{11}$$

where G is the fundamental solution of the unsteady 3D wave equation.

$$G(\boldsymbol{x}-\boldsymbol{y},t-s) = \frac{\delta\left((t-s)-\frac{|\boldsymbol{x}-\boldsymbol{y}|}{c}\right)}{4\pi|\boldsymbol{x}-\boldsymbol{y}|} \tag{12}$$

where δ is delta function. We obtain u at any inside point in the domain using u at boundary points which obtained by equation (11)

$$\begin{aligned}u(\boldsymbol{x},t) = &\int_0^t \int_{\partial D} G(\boldsymbol{x}-\boldsymbol{y},t-s)\frac{\partial u}{\partial n}(\boldsymbol{y},s)d\Gamma ds \\ &- \int_0^t \int_{\partial D} \frac{\partial G}{\partial n}(\boldsymbol{x}-\boldsymbol{y},t-s)u(\boldsymbol{y},s)d\Gamma ds + u_{\text{in}}(\boldsymbol{x},t),\end{aligned} \tag{13}$$

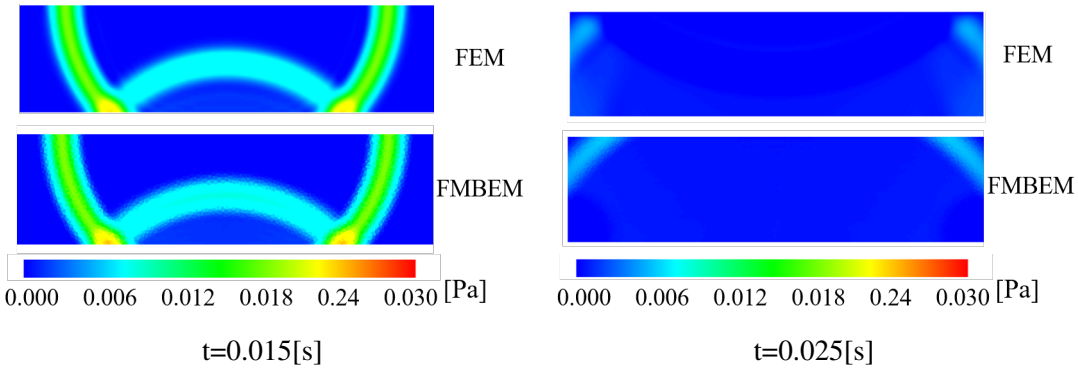

Figure 2: Comparison of sound pressure distribution

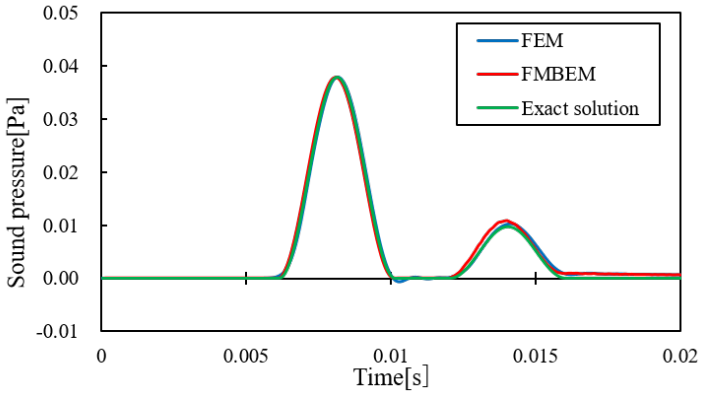

Figure 3: Comparison of sound pressure at the sound receiving point

3 EXAMPLE OF NUMERICAL ANALYSIS

3.1 Benchmark analysis

・Numerical conditions

To verify the validity of the acoustic analysis program using the finite element method, a benchmark analysis is performed using the analysis model shown in **Fig.1**, and compared with the exact solution and the fast multipole boundary element method. Spherical waves from the upper surface of the model and checked the reflection at the lower surface and the effect of sound absorption at the absorption boundary given to the measurement surface. In this analysis, the boundary condition of the lower surface is an impedance boundary condition with a reflectance of 0.5. We set Δx to 0.05m, Δt to 0.01ms, and the incident wave used is the 250Hz cos wave.

・Numerical results

Fig.2 qualitatively confirm that sound is reflected at the lower surface and absorbed at the absorption boundary. **Fig. 3** compares the sound pressure obtained at the sound receiving point with the exact solution. Both analysis results were nearly equal to the exact solution, and relative errors of the maximum values of direct sound and reflection sound in finite element analysis were 0.0098[%], 0.0534[%], and

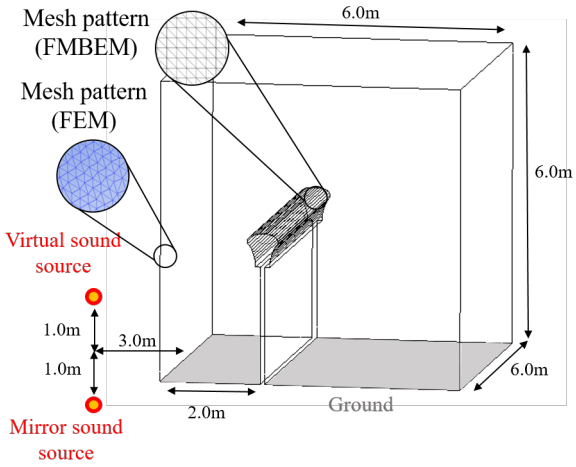

Figure 4: Computational model (mushroom type)

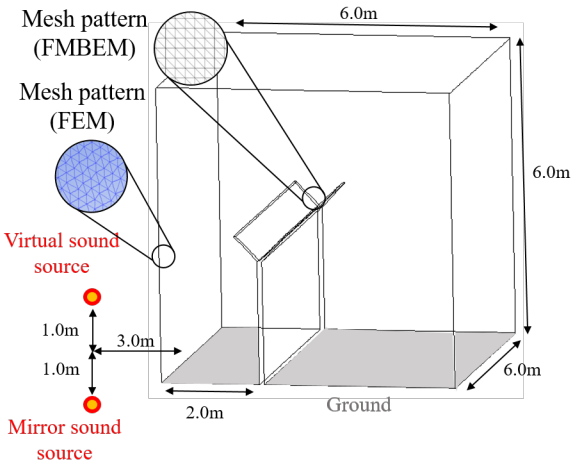

Figure 5: Computational model (Y-shaped type)

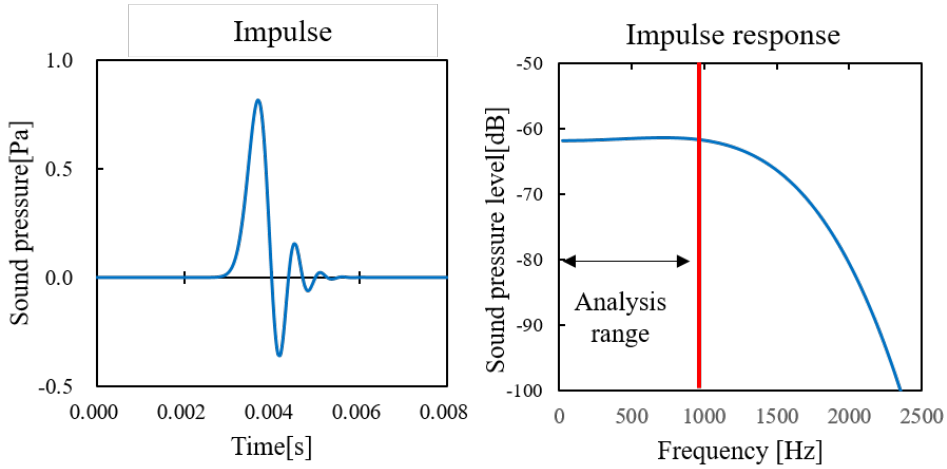

Figure 6: pseudo impulse of Lubich

they in boundary element analysis were 0.0055[%], 0.1157[%]. The finite element method delayed the reach of maximum sound pressure 6.0e-4[s], 4.0e-4[s], however, the boundary element method did not delay because the boundary element method has the fundamental solution.

3.2 Sound barrier analysis

・Numerical conditions

Fig.4 and **Fig.5** shows the analysis model. The computation was performed on three type models, vertical, mushroom type, and Y-shaped sound wall. The model has the elements length of 0.022m, and the time discretization width of analysis is 0.0667ms. Boundary conditions were analyzed in two ways: perfect reflection and 0.5 reflectances. We apply the absorbing boundary condition to the incident boundary surface in the finite element method. The incident wave used the pseudo impulse of Lubich [4] [5]. **Fig.6** shows the time history and frequency response of the pseudo-impulse response generated

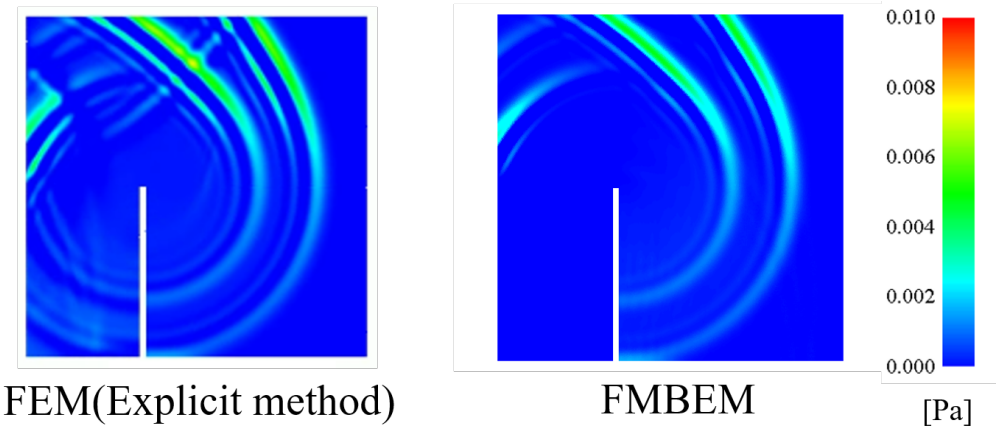

Figure 7: Comparison of sound pressure distribution around a vertical wall (t = 0.0217[s])

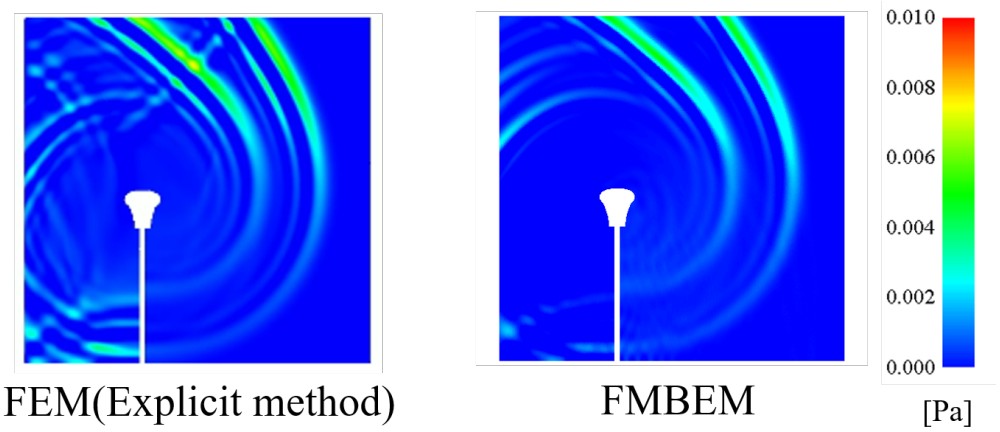

Figure 8: Comparison of sound pressure distribution around a mushroom type wall (t = 0.0217[s])

by the (14). This impulse has a feature that has a constant frequency until a certain section and decays sharply at higher frequencies. This feature means that it prevents from occurring analysis errors by high frequency. The constant frequency response range can be changed by the parameter change in (14). Here, r and Δt are assumed to be r = 1.8m, and Δt = 0.0667ms respectively, the analysis range is until 1000Hz.

$$u(\Delta t) \cong \frac{R^{-n}}{L} \sum_{L=0}^{L-1} \left(\frac{1}{4\pi r} e^{-\frac{s}{c} r} \right) e^{\left(-2\pi i \frac{nl}{L}\right)} \tag{14}$$

To compare the finite element method and the fast multipole boundary element method, analyses were integrated with the element length and the sound barriers. We used ”CrayXC40” which is a super computer system and is possessed by Kyoto university in Japan. This super computer system has 68cores and 90GB of memory in a node. These analyses used 16nodes(1088cores) and performed the parallel calculation.

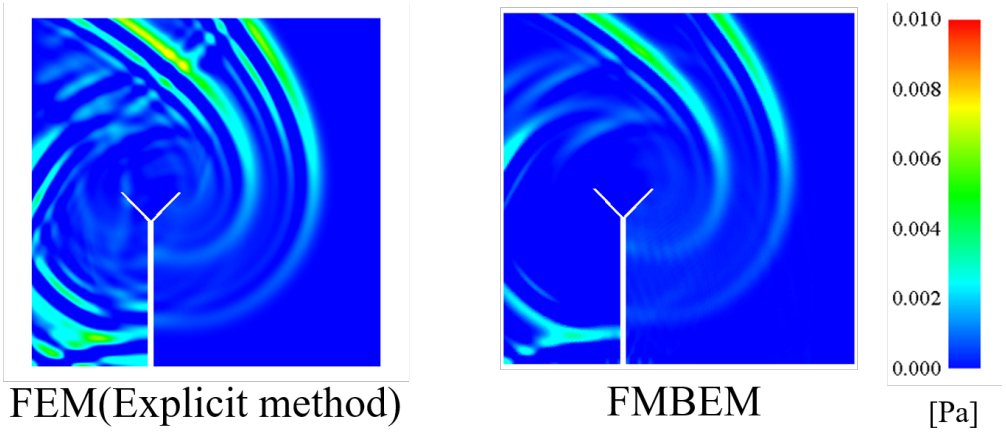

Figure 9: Comparison of sound pressure distribution around a Y-shaped wall (t = 0.0217[s])

Table 1: Comparison of CPU time and memory required

		CPU time	Used memory for mesh data[GB]	Used memory for Calculation[GB]
Perfect reflection	FEM	8.1minute	7.55	46.7
	FMBEM [Boundary calculation]	1.5hour	0.07	73.4
Random reflection	FEM	16.5minute	7.55	49.5
	FMBEM [Boundary calculation]	23.2hour	0.07	90.4

・Numerical results

We found analysis result of the finite element method occurs the direct sound and reflected sound followed by numerical vibrations. **Fig.7** - **Fig.9** shows a comparison of the finite element method and the fast multipole boundary element method for visualization results by types. From the computatinal results, The Y-shaped sound wall can reduce sound pressure a little more than other types. Also, the visualization of the finite element method shows more sound bands than the visualization of the fast multipole boundary element method, and the sound pressure value was higher than that of the fast multipole boundary element method because the sound was not fully absorbed at the absorbing boundary.

A comparison of analysis costs is shown in **Table.1**. The table shows that the finite element method requires less analysis time and computer memory than the boundary element method.

・Auralization

We convoluted the real source sound to the impulse response. Where, the real source sound is the pile-driving sound(**Fig.10**). Also, the results of aulralization projected onto a VR system. The VR device : Holostage and experience is shown in **Fig.11**, **Fig.12**. **Fig.13** and **Fig.14** compare the analysis results with the measured value observed by the VR system. Both results can be confirmed to be in good agreement. Some of the deviations in **Fig.14** are thought to be influenced by the background noise in the VR system.

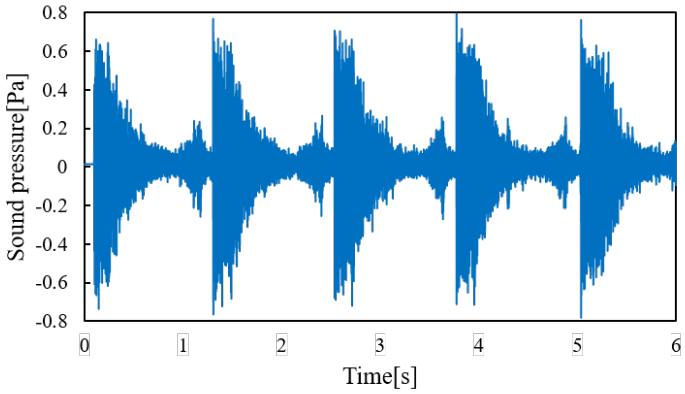

Figure 10: Real sound source (pile-driving machine noise)

We will show at the time of the presentation about auralization results of other sound barrier results and those of the finite element analysis.

4 CONCLUSIONS

In this paper, noise evaluation systems based on finite element method and the fast multipole boundary element method have been presented. The impulse response analysis has been usefully introduced to realize the efficient numerical simulation. The presents methods have been applied to the benchmark problem and the sound field analysis around the sound insulation wall with complicated shape. The noise evaluation system has been also developed for the use of immersive VR device. The computed results are good agreement with the observed results in VR space.

REFERENCES

[1] Takahashi, T. An interpolation-based fast-multipole accelerated boundary integral equation method for the three-dimensional wave equation. *Journal of Computational Physics.* (2014) **258**:809-832.

[2] Nomura, T., Takagi, k. and Sato, S. Finite element simulation of sound propagabion concerning meteorological conditions. *International Journal for Numerical Methods in Fluids.* (2010) **64**:1296-1318.

[3] Mur, G. Absorbing boundary conditions for the finite difference approximation of the time-domain electromagnetic-field equations. *IEEE Transactions on Electromagnetic Compatibility.* (1981) **23**:377-382.

[4] Lubich, C. Convolution quadrature and discretized operational calculus. I. *Numerische Mathematik.* (1988) **52**:129-145.

[5] Lubich, C. Convolution quadrature and discretized operational calculus. II. *Numerische Mathematik.* (1988) **52**:413-425.

Figure 11: VR system

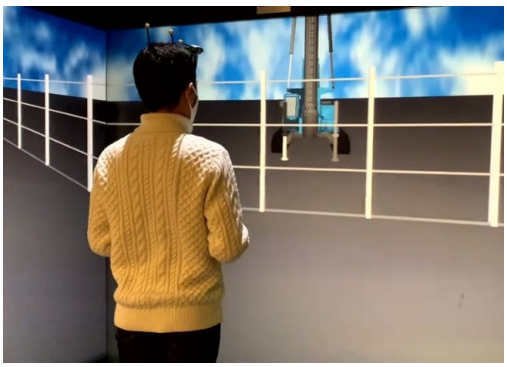

Figure 12: Scene of auralization in VR space

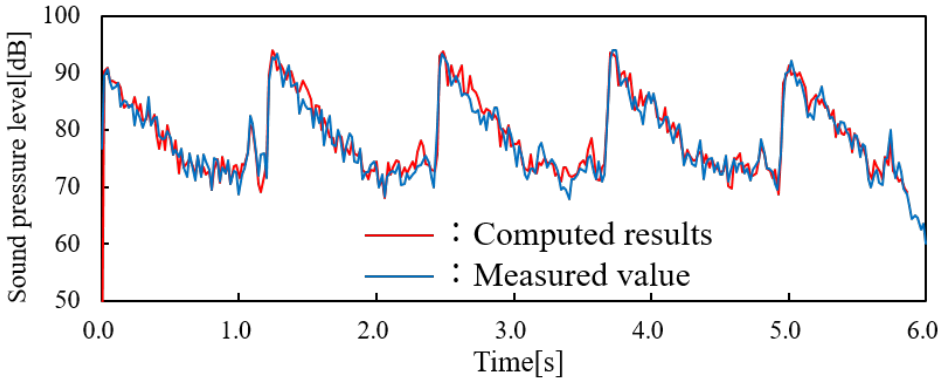

Figure 13: Comparison of sound pressure level(no sound wall)

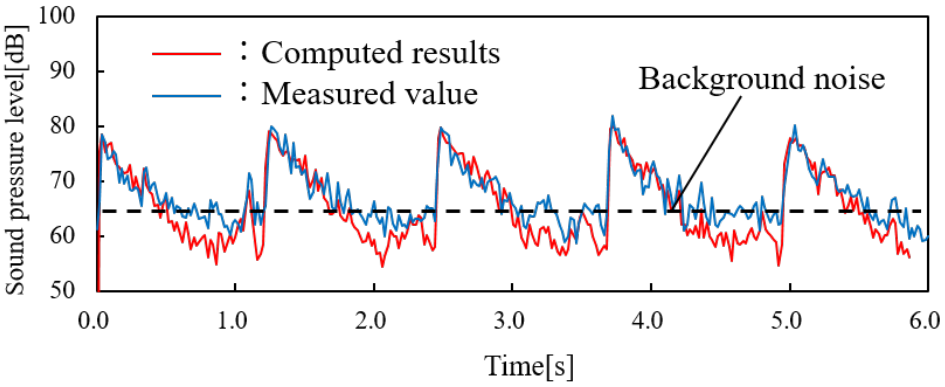

Figure 14: Comparison of sound pressure level(vertical sound wall)